Real-Time Mandibular Angle Reduction Surgical Simulation With Haptic Rendering

Qiong Wang, Hui Chen, Wen Wu, *Member, IEEE*, Hai-Yang Jin, and Pheng-Ann Heng, *Senior Member, IEEE*

***Abstract*—Mandibular angle reduction is a popular and efficient procedure widely used to alter the facial contour. The primary surgical instruments, the reciprocating saw, and the round burr, employed in the surgery have a common feature: operating at a high speed. Generally, inexperienced surgeons need a long-time practice to learn how to minimize the risks caused by the uncontrolled contacts and cutting motions in manipulation of instruments with high-speed reciprocation or rotation. A virtual reality-based surgical simulator for the mandibular angle reduction was designed and implemented on a compute unified device architecture (CUDA)-based platform in this paper. High-fidelity visual and haptic feedbacks are provided to enhance the perception in a realistic virtual surgical environment. The impulse-based haptic models were employed to simulate the contact forces and torques on the instruments. It provides convincing haptic sensation for surgeons to control the instruments under different reciprocation or rotation velocities. The real-time methods for bone removal and reconstruction during surgical procedures have been proposed to support realistic visual feedbacks. The simulated contact forces were verified by comparing against the actual force data measured through the constructed mechanical platform. An empirical study based on the patient-specific data was conducted to evaluate the ability of the proposed system in training surgeons with various experiences. The results confirm the validity of our simulator.**

***Index Terms*—Haptic rendering, impulse-based dynamics, mandibular angle reduction, surgical simulation evaluation, surgical simulation.**

I. Introduction

MANDIBULAR angle reduction [1] is the most common and popular procedure to remodel the facial contour. It alters the shape of mandibular angle to turn the patient from a wide lower face to an oval or a slender one. It has been reported in many medical investigations [2] that this surgery can efficiently reduce the width of the face in the frontal view as well as the curvature of the mandible in the lateral view. This procedure employs two basic strategies [3]: 1) the linear mandibular angle ostectomy using a reciprocating saw, shown on the bottom of Fig. 1(b), to dramatically remove protruding part and change the mandible outline. The ostectomy cutting line is illustrated in the dotted line in Fig. 1(a); 2) the mandibular angle ridges or sharp angles smoothing using a round burr, shown on the top of Fig. 1(b), to create a natural curvature between the osteotomy part and ramus posteriorly, or body anteriorly. The regions needed to be burred are marked in solid lines in Fig. 1(a).

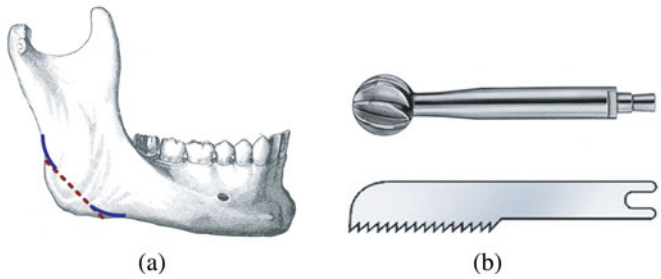

Fig. 1. Mandibular angle reduction: (a) illustration of marks for mandibular angle reduction and (b) surgical instruments used in the procedure.

A safe and successful procedure requires surgeons to have a high level of skill in handling the electric instruments of reciprocating saw and round burr to perform precise bone cutting and burring. Mishandling of these instruments may cause severe complications [4], [5] during or after the surgery, such as damage to the inferior alveolar nerve or fracture on the ramus of mandible body. Surgeons therefore need to undergo extensive practice in manipulating these electric instruments. In comparison to the traditional training methods on plastic or synthetic models, animals, cadavers and patients, virtual reality (VR)-based surgical training with force feedback is a safe and feasible alternative. It allows the user to perform a variety of manipulation tasks easily and repeatedly.

The development of a realistic simulator with interactive components for mandibular angle reduction is a challenging task. The surgical instruments used in the procedure, reciprocating saw and round burr, are both electric motor-driven equipments and work at high reciprocation or rotation speeds. Currently available orthopaedic surgery simulators allow for interactive manipulation of various instruments, such as burr, drill, and saw [6]. In these simulators, the haptic modeling of the sawing and burring operation was generally built on the simplified

Manuscript received December 15, 2011; revised April 11, 2012 and July 5, 2012; accepted September 4, 2012. Date of publication September 10, 2012; date of current version November 16, 2012. This work was supported by the National Fundamental Research Grant of Science and Technology under 973 Project 2009CB320804, the National Natural Science Foundation of China under Grant (NSFC 61135003, 61175124), and the Multiyear Research Grant of the University of Macau under Grant MYRG150(Y1-L2)/FST11/WW.

Q. Wang is with the Department of Computer Science and Engineering, The Chinese University of Hong Kong, Shatin, Hong Kong (e-mail: qwang@cse.cuhk.edu.hk).

H. Chen is with the Intelligence Engineering Lab, Institute of Software, Chinese Academy of Sciences, Beijing 100864, China (e-mail: chenhui@iscas.ac.cn).

W. Wu is with the Department of Computer and Information Science, University of Macau, Macau 999078, China (e-mail: WenWu@umac.mo).

H.-Y. Jin is with the Shenzhen Institutes of Advanced Technology, Chinese Academy of Science, Shenzhen 518055, China and also with the Shenzhen Graduate School, Harbin Institute of Technology, Shenzhen 518055, China (e-mail: hy.jin@sub.siat.ac.cn).

P.-A. Heng is with the Department of Computer Science and Engineering, The Chinese University of Hong Kong, Shatin, Hong Kong, and also with the Shenzhen Institutes of Advanced Technology, Chinese Academy of Science, Shenzhen 518055, China (e-mail: pheng@cse.cuhk.edu.hk).

Color versions of one or more of the figures in this paper are available online at http://ieeexplore.ieee.org.

Digital Object Identifier 10.1109/TITB.2012.2218114

model [7], the estimation with elastic theory [8], or the metal machining theorem [9]. Some problems still need to be resolved. The material properties and the high speed were not considered in the model of [7]. The geometry information at contact was ignored in [8]. In [9], multiple parameters were determined through complicated experiments. The torque feedback of the bone drilling was discussed in [9], however, the torque effect of the bone sawing has not been reported in any publications to our best knowledge. For surgical simulators with haptic rendering, another difficult task is the haptic force evaluation.

In this paper, a surgical simulation system integrated with interactive bone-sawing and bone-burring processes for the mandibular angle reduction was developed on a CUDA-based platform. The immersive training environment for surgeons to perform mandibular angle reduction is presented with both visual and haptic feedbacks. Our study reflects the inclusion of haptic feedback in the emulation of the surgical instruments and their interaction with a computer-generated model. The contributions are summarized as follows:

1) Haptic forces and torques generated on the motor-driven high-speed instruments were computed using the impulse-based dynamics. By tracing the translational motions and rotations or reciprocations of the instruments at contact, the contact forces under two friction modes, static and dynamic modes, were calculated. In particular, the torques caused by the improper manipulation of the reciprocating saw during cutting operation were considered in our model, that was used to guide users for the better control of the saw.
2) A mechanical platform was constructed to measure the actual forces produced by the bone-sawing and bone-burring operations. A series of sawing and burring operation tests on fresh bovine bone samples was carried out under controlled conditions on the platform, and the recorded forces were compared with the simulated forces.
3) The patient-specific data before and after mandibular angle reduction were used to evaluate the capability of the proposed system in training surgeons with various experiences. Differences of cephalometric values of gonial angle (GA) and manidublar plane angle (MPA) to the Frankfort horizontal plane between the simulated results and the actual surgical results were compared. The completion time of users to perform the whole ostectomy procedure and the percentage of the torque exceeding the threshold were recorded as the statistics for determining a learning curve in training novice people. The results showed that the proposed system can efficiently mimic the mandibular angle reduction procedure.

The rest of the paper is organized as follows: Section II introduces the related previous work. Section III shows the overview of the whole system. Section IV presents the haptic models during the interaction, including the saw force modeling, the sawing torque constraint, and the burring force modeling. Section V presents bone reconstruction and refinement method. The evaluation of the haptic models and the analysis of the empirical study of the proposed mandibular angle reduction simulator are presented in Section VI. The conclusion is given in Section VII.

II. Related Work

In this section, we briefly overview the previous related work especially in orthopaedic surgery simulation systems with haptic feedback and the evaluation methods about the virtual surgery.

Recently, several surgery simulation systems with suitable haptic feedback models to increase the realism of the orthopaedic surgery simulation have been investigated. Morris *et al.* [6] developed a high-fidelity visuohaptic bone-drilling simulation system. The tangential force acting on the instrument was modeled based on the volumetric sampling of the haptic drill. The tangential force at each sampled point was scaled following the velocity at this point. Pflesser *et al.* [7] presented a virtual petrous bone surgery system incorporating a drill-like tool to perform successive cutting operation on multivolume data. In their work, a proxy-based Hooke's law was introduced to simulate the haptic interaction between the cutting tool and voxel-based bone data. In their model, material properties and various velocities of the tool that greatly affect the contact force in the real surgery were inaccessible. Agus *et al.* [8] constructed a virtual surgical system to train the skill of burring temporal bone. Hertz's contact theory was applied to evaluate the haptic forces and the bone-erosion process of the bone-burring interaction. Their haptic model involved the penetration depth between interactive objects, the elastic properties of the contact bodies, and the shape of the contact area. However, the geometry and the characteristic of the instrument at contact were ignored. Taking the symmetrical shaped round burr as an example, the sensation of burring the bone with its tip area should be different from burring with its equator area, because the burr has complicated geometry and works by rotational motion. Hsieh *et al.* [9] integrated an interactive oscillating bone-sawing simulation into a linear osteotomy of the femur amputation. The sawing force acting on the saw teeth was computed based on the machining theorem [10] with parameters including feed rate, oscillating speed, saw length, and geometry. However, these parameters were determined through complicated experiments.

In our paper, a haptic model is proposed to analyze the physical contact between the electronic instruments and the bone material. The contact geometry, material properties, and velocities are explicitly included. These parameters can also be conveniently tuned by users to fit various surgical situations.

As various surgical simulators are increasingly produced, the methodologies to evaluate the simulators have been attracting a lot of attentions and have been widely discussed [11]. Hariri *et al.* [12] reported the method to evaluate a surgical simulator of learning clinical anatomy. They separated users with the same anatomy cognition ability into two groups, one was to learn the human anatomy from the textbook (taking as an good learning approach) and the other was to learn using the surgical simulator. The mean identification scores served as the objective performance metrics. It was recorded and compared to demonstrate learning with surgical simulator obtained same results as textbooks, thus verifying the effectiveness of the simulator. Furthermore, statistical data analysis was introduced to analyze the performance score data. For example, Grantcharov *et al.* [13] invited experienced and inexperienced surgeons to train on the developed laparoscopic surgical simulator. Statistical data analysis was performed to examine the score of these two groups. A learning curve could be found in the inexperienced surgeons

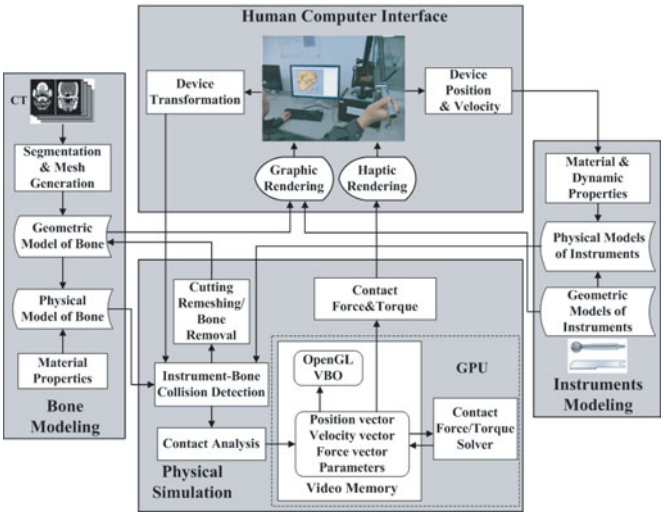

Fig. 2. Framework of the proposed simulator.

group, while it was missing from the group of experienced surgeons. This demonstrated the simulator was valid and could distinguish surgeons from varying surgical levels. This evaluation method was also used in [14] and [15]. Some other evaluation methods adopted subjective performance metrics, in which the user completed a questionnaire to assessing the reality of the system's external appearance, the simulation of procedures and so on, such as work in [16] and [17].

In our paper, the evaluation consists of two parts. First, a mechanical platform was constructed to validate the haptic force generated in our virtual surgery system. Then, the patient-specific data before and after the real mandibular angle reduction surgery were adopted in the empirical study as the benchmark of the objective performance metrics.

III. System Overview

The proposed simulator is divided into four modules (see Fig. 2): bone modeling, instrument modeling, physical simulation, and human–computer interface. The bone-modeling module is responsible of the preprocessing of mandible data segmentation and triangular mesh reconstruction. The bone regions were automatically segmented by insight segmentation and registration toolkit on a full-head computerized tomography (CT) data of the patient. The triangular mesh of the mandible was reconstructed by Marching Cubes algorithm [18]. To construct the physical model of the mandible, properties of the individual material were assigned to each vertex of the geometric model. In this paper, we assume that the bone material is uniform. Therefore, all the vertices have the same material property. However, our model can be easily expanded to apply on the bone model with different kind of materials by distributing vertices with distinct haptic properties. Similarly, we constructed the physical models of the reciprocating saw and round burr. In addition, the dynamic properties of the instruments, such as linear velocity, reciprocating frequency or angular velocity were assigned to the physical models of instruments. In the physical simulation module, the proposed haptic models were processed with the CUDA-based platform on graphics processing unit (GPU). This can increase the computational efficiency of the forces and torques and maintain the stability of the refresh rate of the haptic feedback. In the computation of the feedback force and torque, the position, velocity, and force vectors of all sampled points on the instruments were initialized, and transferred to the interface class that allocated the global video memory for them. The contacts were checked between the instruments and bone model iteratively at a certain speed. If contact occurred, the configurations at contact, including the size and the shape of the intersection area and various velocities, were delivered to the contact analysis function. The contact force and torque solvers (kernels) in GPU received the velocity changes caused by the contact. Afterward, the corresponding kernels were launched to calculate the new position, velocity, and force vectors. The interactive force and torque were evaluated and transmitted to the haptic device for haptic rendering. A real-time bone remeshing and refinement method was also included in this module. The human–computer interface managed the transformation from the haptic-device coordinates to the bone–model coordinates and recorded the position and translational velocity of the stylus tip of the device.

IV. Haptic Interaction

The bone surgical instruments are the motor-driven high-speed bodies. Therefore, it is more difficult to model the haptic interactions between the instruments and the rigid material. The haptic feedback model derived from the impulse-based dynamics in our previous work [19] was integrated and extended in this study to compute the forces and torques during the interactions.

A. Bone-Instrument Description

In a typical operation, the reciprocating saw moves forward and backward repeatedly at a frequency of 15 000 TPM (times per minute). The round burr works at a high rotational speed of approximate 50 000 r/min. The contact force can be obviously felt during the penetrations into the rigid bone. Thus, it is crucial to integrate the high-speed component into the force-feedback modeling.

To integrate the high-speed component, impulse-based dynamics [20] was used to compute the contact forces between the instruments and the bone material. This method can easily process the velocity changing of the colliding objects at the contact, thus it is convenient to handle the high velocities of the instrument during the feedback-force computation. In this paper, we expanded our previous work [19] about haptic bone-burring model to support both sawing and burring models. During the simulation, the rigid bone model is considered a static object with infinite mass. Basically, the contact forces applied on the instruments during the interactions with the bone are handled in the following ways.

1) Since the main contact forces are generated on the cutting edges of the instrument, the cutting edges are sampled during collision detection. The sampled points distributed uniformly on the edges are used in checking the contacts with the bone model. Individual contact force is first computed at each sampled point, and then summed up.
2) It is required to identify various velocities of the sampled points involved in the contact. The translational velocity,

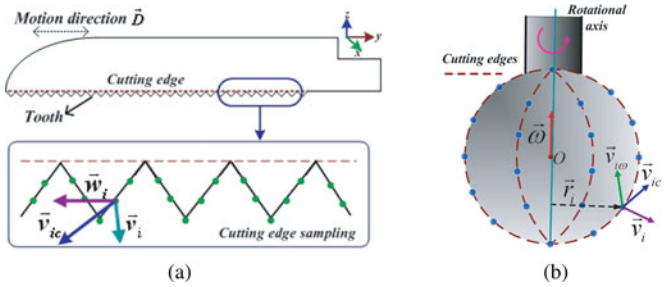

Fig. 3. Haptic modeling.

which can be obtained through the haptic device, is the velocity that the user manipulates the instrument. Self-reciprocation or self-rotation of the instruments are the motor-driven velocities, which are assigned as parameters of the saw or burr instruments.

3) Contact forces simulated by the impulse-based haptic model have two distinct modes: the static friction mode and dynamic friction mode.

B. Impulse-Based Haptic Models

1) Sawing Force Modeling: As shown in Fig. 3(a), the reciprocating saw moves forward and backward along the *Y*-axis during the operation, and the current motion direction is represented by $\vec{D}$. Moreover, the reciprocating saw consists of many teeth on the cutting edge. The cutting edge was uniformly sampled on these teeth, which were indicated by the circular points in Fig. 3(a). The saw blade is assumed extremely thin and the thickness is ignored in the modeling. Each sampled point has its translational velocity $\vec{v}_i$ and the velocity caused by the reciprocating motion of the saw $\vec{w}_i$ can be computed as $\vec{w}_i = 4AF\vec{D}$. Here, A and F are input parameters of the reciprocating amplitude and frequency, respectively. Since there are angles between the teeth on the saw blade and the bone surface, the motion along $\vec{w}_i$ can break and split the bone material easily. While operating the reciprocating saw, the translational velocity of the saw is expected to follow the original incision plane to avoid the accidental fracture of the bone. In this section, we suppose $\vec{v}_i$ is always following the original incision plane and the other situations will be discussed in the next section. Therefore, the compound velocity at each sampled point can be represented as $\vec{v}_{ic} = \vec{v}_i + 4AF\vec{D}$.

Positions at a sampled point in two consecutive time steps are connected as a segment. Ray collision [21] is used to determine the contact between this segment and the bone mesh model. If a contact is detected, the sampled point at the instrument and the corresponding interaction point on the bone mesh are retrieved. The contact normal $\vec{N}_i$ is assigned as the linear interpolation of the normals of the contacted triangles on the bone mesh. If the sampled point satisfies $\vec{w}_i \cdot \vec{N}_i > 0$, then this point does not contribute to the sawing force computation.

Contact forces with the static friction mode and dynamic friction mode are considered. Suppose p_i is the contact impulse at the contact point. If p_i is within the friction cone, that is $|\vec{p}_i - (\vec{p}_i \cdot \vec{N}_i)\vec{N}_i| \leq \mu\vec{p}_i \cdot \vec{N}_i$, the contact force is in static friction mode, otherwise it is computed in dynamic friction mode. Here, μ is the friction coefficient and set to 0.3 [22].

In static friction mode, the contact impulse applied on the contact point is computed according to impulse-based dynamics [20] with

$$\vec{p}_i = K_i^{-1}(\vec{u}_{\mathrm{ic}} - \vec{v}_{\mathrm{ic}}) \tag{1}$$

where K_i is a collision matrix at the contact point and can be calculated according to $K_i = \frac{1}{M}I + r_i^* J^{-1} r_i^*$, M is the mass of the saw, I is the identity matrix, J is the inertia tensor of the saw, and r_i^* is the cross-product matrix of the vector from the contact point to the centroid of the instrument. $\vec{u}_{\mathrm{ic}}$ is the compound velocity after the contact, with the form $\vec{u}_{\mathrm{ic}} = -e(\vec{v}_i + 4AF\vec{D})$ according to Newton's impact law. e is the composite coefficient of restitution and can be computed using the Young's Modulus and Poisson's Ratio with the method in [23], which was 0.6.

In dynamic friction mode, the contact impulse is derived according to impulse-based dynamics and Newton's impact law [24]

$$\vec{p}_i = \frac{-(e+1)(\vec{v}_i + 4AF\vec{D})(\vec{N}_i - \mu\vec{T}_i)}{\vec{N}_i^T K_i(\vec{N}_i - \mu\vec{T}_i)} \tag{2}$$

where $\vec{T}_i$ is the normalized vector consistent to the direction of the compound velocity $(\vec{v}_i + 4AF\vec{D})$ and $\vec{N}_i^T$ is the transposition of $\vec{N}_i$. Given the contact impulse, the contact force f applied on the saw blades can be evaluated according to the impulse-momentum theorem

$$\vec{f} = \sum_i \vec{f}_i = \sum_i \frac{\vec{p}_i}{\Delta t} \tag{3}$$

where Δt is the time duration of the contact and $\vec{f}_i$ is the force applied on the contact point.

2) Sawing Torque Constraint: Rotating the instrument during sawing operation is considered as a dangerous action. It is inclined to cause mandible fracture, especially to the patients with thin mandible or osteoporosis [25]. Also, it greatly increases the possibility of the saw blade breakage. In order to avoid the bone fracture and guide the user to perform the sawing operation with appropriate posture, a warning message is prompted if the torque caused by the incorrect rotation of the saw exceeds a predefined threshold.

Considering that the torque is generated because the saw blade is unintentionally rotated along the *Y*-axis when it is moved in the original incision plane by the user, as shown in Fig. 4(a). Therefore, there is an angle α as illustrated in Fig. 4(b), between the incision plane and the saw blade plane. Contacts occur between the bone and the back edge of the saw blade during sawing operation. The sampled contact points are illustrated in square point in Fig. 4(a). The contact force at point j is denoted as $\vec{f}_j$. It can be computed with the impulse-based dynamics according to (3). $\vec{f}_j$ is decomposed into two components according to the saw blade plane, as shown in Fig. 4(a): $\vec{f}_{\mathrm{jn}}$ is normal to the saw blade plane; $\vec{f}_{\mathrm{jt}}$ lies in the saw blade plane. The two corresponding torques are calculated by the following equations:

$$\vec{\tau}_{\mathrm{jn}} = \vec{l}_j \times \vec{f}_{\mathrm{jn}}, \quad \vec{\tau}_{\mathrm{jt}} = \vec{l}_j \times \vec{f}_{\mathrm{jt}} \tag{4}$$

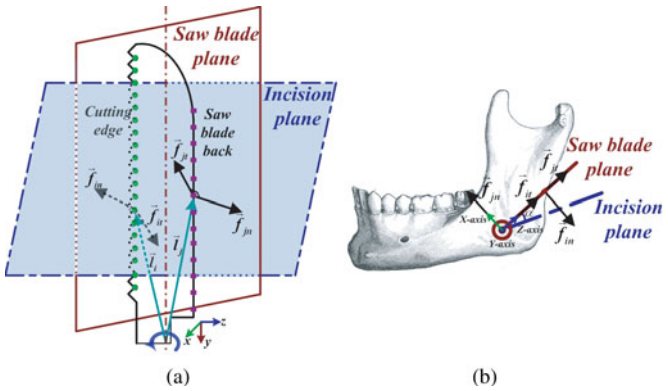

Fig. 4. Torque modeling during the slight rotation of the saw blade around the long axis of the saw.

where $\vec{l}_j$ is the vector from the point that the torque is measured to the jth contact point on the back of the saw blade. Moreover, the torque applied on the cutting edges of the saw blade can be handled by the same decomposition

$$\vec{\tau}_{\rm in} = \vec{l}_i \times \vec{f}_{\rm in}, \quad \vec{\tau}_{\rm it} = \vec{l}_i \times \vec{f}_{\rm it}. \tag{5}$$

Similarly, $\vec{l}_i$ is the vector from the point that the torque is measured to the ith contact point on the cutting edges, $\vec{f}_{\rm in}$ is the force normal to the saw blade plane at ith contact point on the cutting edge, $\vec{f}_{\rm it}$ is the force component in the saw blade plane. Then, the torque applied on the saw blade during its rotation along the *Y*-axis can be computed

$$\vec{\tau}_{r,n} = \sum_j \vec{\tau}_{\rm jn} + \sum_i \vec{\tau}_{\rm in}, \quad \vec{\tau}_{r,t} = \sum_j \vec{\tau}_{\rm jt} + \sum_i \vec{\tau}_{\rm it}. \tag{6}$$

According to the right-hand screw rule, $\vec{\tau}_{r,n}$ works in the saw blade plane. It has the tendency to rip the saw blade. Hence, this part will not cause the fracture of the bone material during the sawing operation and is ignored. $\vec{\tau}_{r,t}$ is perpendicular to the saw blade plane, which acts on the bone material vertically. If $\vec{\tau}_{r,t}$ becomes too large, the fragile bone piece will likely be broken up. Therefore, surgeons need to avoid imposing large torque caused by the improper manipulation of the saw on the mandible during sawing. In our system, a threshold was set to have the dangerous torque of $\vec{\tau}_{r,t}$ under control. Our system will prompt a warning message if the torque is larger than the threshold. This function helps the user keep the stability of a sawing trajectory along the original incision plane.

3) Burring Force Modeling: As shown in Fig. 3(b), the round burr rotates in an angular velocity of $\vec{\omega}$ along the axis illustrated with the solid line. The cutting blades are illustrated by the dashed lines with the sampled points on the round burr head. At each sampled point, the translational velocity $\vec{v}_i$ and the velocity caused by angular velocity $\vec{v}_{i\omega}$ need to be obtained first. The compound velocity at each point is decomposed at the contact normal $\vec{N}_i$. Then, the contact force can be computed following the impulse-based dynamics. Here, only the final equations computing the impulses and the force are given, For the detailed derivation, please refer to our paper [19].

In static-friction mode, the contact impulse is

$$\vec{p}_i = K_i^{-1}(-e(\vec{v}_i + \vec{\omega} \times \vec{r}_i) - \vec{v}_{\rm ic}). \tag{7}$$

Similarly, $K_i = \frac{1}{M} I + r_i^* J^{-1} r_i^*$, but in the burring-force model, M and J are the mass and the inertia tensor of the burr, respectively, r_i^* is the cross-product matrix for the vector from the contact point to $\vec{O}$.

In dynamic-friction mode, the contact impulse can be computed as

$$\vec{p}_i = \frac{-(e+1)(\vec{v}_i + \vec{\omega} \times \vec{r}_i)(\vec{N}_i - \mu\vec{T}_i)}{\vec{N}_i^T K_i (\vec{N}_i - \mu\vec{T}_i)} \tag{8}$$

where $\vec{N}_i^T$ is the transposition of $\vec{N}_i$. The final force applied on the burr can also be estimated

$$\vec{f} = \sum_i \frac{\vec{p}_i}{\Delta t}. \tag{9}$$

In comparison with the torque generated by the gripping force of the user, the torque applied during the burring operation is ignored.

V. Real-Time Bone Removal and Reconstruction

Simulating the sawing, cutting, and burring operations implies a modification of a simulated bone structure over time. In our simulation, a simplified bone removal and reconstruction method is carried out to implement the real-time topological changing of the bone structure.

The remeshing of bone model during the sawing operation includes two parts: one part is to generate a mesh surface at the cross section swept by the saw blade; the other is to reconstruct the original surface of the mesh model cut by the saw blade. The cutting blade is decomposed into several small segments. The real-time position of the blade, called the cutting front, is represented with a point sequence $\{C_1^i, C_2^i, \ldots, C_n^i\}$, where i denotes the time sequence and n represents the number of points, which can be adjusted by the user according to the resolution of the bone mesh.

To reconstruct the bone model, we triangulate two consecutive cutting fronts. Each four neighboring points, for example, $C_k^i, C_{k+1}^i, C_k^{i+1}, C_{k+1}^{i+1}$, can form two triangles. The surface formed by those triangles is called the swept surface. As shown in Fig. 5(a), the cutting front is illustrated in the dashed line and the triangles in solid lines demonstrate the swept surface within three time steps.

At each time step, ray collision detection is performed to check the interaction between edges of the swept surface and the original bone mesh. The interaction points are shown in Fig. 5(a) in circular points. The interaction points between the edges of the original bone mesh and the swept surface are also determined, which are illustrated with square points in Fig. 5(a).

With these two kinds of intersection points, the bone model is remeshed using a 2-D polygon triangulation algorithm [26]. For the mesh generation of cross section swept by the blade, the 2-D triangulation algorithm is used to generate the new triangles within the triangle of the swept surface, which has two kinds of interaction points. If three vertices of a triangle on the swept surface are inside the original bone model, this triangle will serve as a part of the new generated mesh of the cross section. The triangles marked in dotted lines in Fig. 5(b) demonstrate the new generated mesh at the cross section swept by the cutting front.

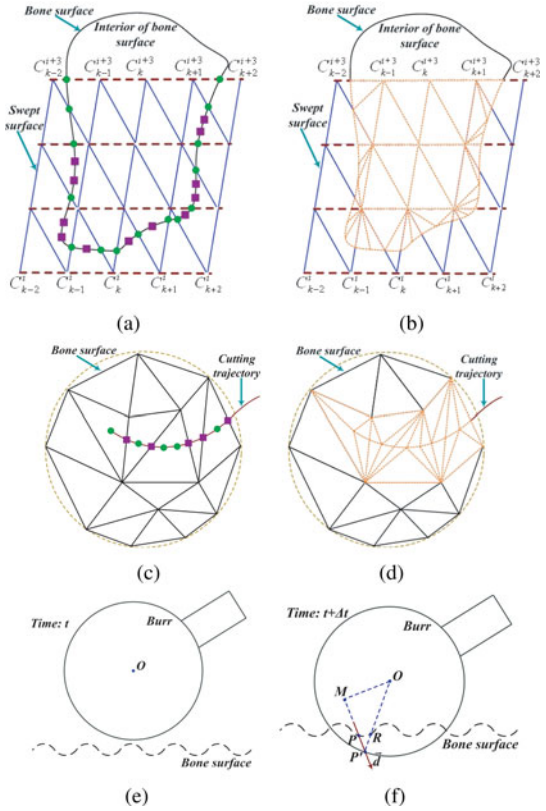

Fig. 5. Bone removal reconstruction methods: (a) and (b) show the generation of a mesh surface at the saw blade cutting cross section, (c) and (d) demonstrate the remesh of the original surface cut by the saw blade, and (e) and (f) show the surface deformation at burring.

For the cutting on the original bone mesh, as shown in Fig. 5(c), the triangles marked in solid lines illustrate a part of the original bone mesh surface, which is cut by the cutting front. The cutting trajectory is illustrated in Fig. 5(c), too. First, the two kinds of interaction points need to be collected and the 2-D triangulation algorithm is used to reconstruct the original surface cut by the saw blade. Fig. 5(d) illustrates reconstructed triangles cut by the saw blade in dotted lines.

For the bone removal in the simulation of burring operation, a simple mesh reconstruction method [19] is used to generate a new mesh surface within the removed bone region. As shown in Fig. 5(e) and (f), the contact of the burr on a bone is represented by two successive instants, time t and $t + \Delta t$. At t, the burr has not contacted the bone surface yet, and in the next time step of $t + \Delta t$, the burr is interacting with the bone. The accumulation of the opposite normals of all vertices within the contact area is calculated and set as direction $\vec{d}$. As shown in Fig. 5(f), the new position of each vertex can be reset along $\vec{d}$.

The reconstructed mesh in sawing and burring simulation is further refined based on a local adaptive Loop subdivision scheme [19], [27]. If the dihedral angle between the normal vectors of two adjacent triangles is larger than a given threshold, the triangles are subdivided. The new positions of the vertices for each subdivided triangle are computed with the principles of the Loop scheme. Therefore, the sharp angles and ridges of the reconstructed mesh become smooth.

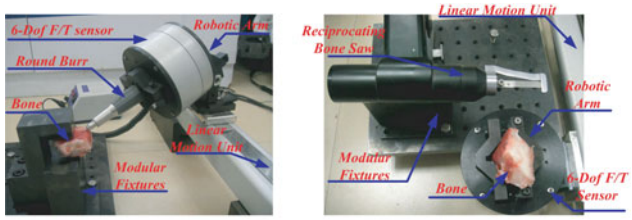

Fig. 6. Mechanical platform for measuring bone-sawing and bone-burring forces.

VI. Experimental Results

Our system of the virtual mandibular angle reduction was performed on a dual-processor Pentium IV/3.0 GHz with 2.0 GB RAM. The graphic card is Nvidia GeForce GTX260 with 2.0 GB video memory. The haptic device is PHANToM Premium 1.5, which can provide 7-DoF positional sensing and 6-DoF haptic feedback. Software configuration includes Visual C++ 2005 and CUDA 2.1 library for graphic rendering, and OpenHaptics Toolkit for haptic rendering.

The performance of the system was sufficient to meet the time constraints for graphic rendering (30 Hz) and force feedback (500–1000 Hz), even though the computational and visualization platform was constructed by affordable and widely used hardware. Currently, the model scale handled by our system was around 8000 triangles. The sampled points on haptic burr were 110 and the sampled point on haptic saw were 86.

A. Haptic Feedback Evaluation

1) Mechanical Platform Setup: In order to validate the proposed simulator, a mechanical platform, as shown in Fig. 6, was constructed to measure the real forces produced by bone-sawing and bone-burring operations. The platform is composed of the following key parts:

1) a robotic arm with 2 DoF used to clamp the instruments and adjust their orientations;
2) a 6-DoF force/torque (F/T) sensor with the force range of ± 20 N and torque range of ± 1.25 Nm;
3) a linear motion unit carrying the robotic arm and used to precisely control the movement of the instrument;
4) a round burr with 4.0-mm diameter and six cutting blades, and a reciprocating bone saw with the blade length of 5.0 cm, commonly used for surgical training;
5) several modular fixtures to fix the bone sample.

The platform was designed to support the measurements of generated forces on the burr and the saw. However, the installations of these two instruments were slightly different. As shown in Fig. 6(a), since the radius of the handpiece of the round burr is comparatively small, it was clamped on the robotic arm and then its movement followed the linear motion unit. The bone piece was fixed and the force applied on the burr was recorded. However, the handpiece of the reciprocating bone saw is generally thick. Therefore, inversely the saw instrument was fixed and the bone piece on the robotic arm was clamped, as illustrated in Fig. 6(b). Then, the force applied on the bone was recorded.

2) Comparison of the Measured and Simulated Forces: To illustrate the effect of the haptic forces of our model in response to high speeds, a series of sawing and burring operation tests on bone samples was carried out under controlled conditions by our constructed mechanical platform. The bone samples were obtained from fresh bovine, because it resembles human bone in structure and mechanical properties [28].

The following strategies were used to obtain the sawing and burring forces. In the sawing test, the reciprocating saw was fixed by the modular fixtures. The bone sample was attached to the robotic arm on the linear motion unit, moved at a constant speed of 0.5 mm/s to contact the saw blade. During the sawing operation, the blade was kept horizontal and gradually cut into the bone sample. With this experimental condition, three sawing operations on the same sample were performed under different reciprocating speeds. The cutting position for each test on the bone sample was close to each other. From the lower to the higher curve as illustrated in Fig. 7(a), the three lines demonstrate the sawing forces at reciprocating velocities of 8000, 10 000, and 15 000 TPM, respectively.

In the burring test, the linear motion unit carrying the robotic arm with the round burr fixed on it was programmed to move at a constant translational velocity of 0.5 mm/s. The head of the round burr was positioned to contact with the flat bone surface with a constant immersive depth of 1.0 mm. The orientation of the burr was fixed during the operation. Under this experimental condition, the tests were carried out for three times with different angular velocities of the burr. From the lower line to the higher one as illustrated in Fig. 7(c), the three lines demonstrate the burring forces at angular velocities of 15 000, 22 000, and 30 000 r/min, respectively. The virtual sawing and burring operations were also performed by the proposed surgical simulator with the same parameters. The measured sawing and burring forces are shown in Fig. 7(b) and (d).

In Fig. 7(a) and (b), the sawing forces were observed to decrease with the increase of the reciprocating speed of the saw instrument. This feature is also consistent with the situation of a real surgery. A surgeon generally feels that the saw is blunt when cutting at a low reciprocating velocity and it is hard to cut off the bone at low reciprocating speed due to the huge resistance in contact. Meanwhile, the force values observed in the sawing force data gradually rise from the beginning of the sawing operation, and then the force values become steady and level off. It is because the sawing blade gradually feeds into the bone sample and the interactive area between the saw blade and the bone material becomes larger. This feature also exists in the simulated sawing force data in Fig. 7(b).

In Fig. 7(c), the measured force in the experiment decreases with the increase of the angular velocity of the burr instrument. This feature can also be found in the simulated force recorded in Fig. 7(d). It is similar to the situation reported in a previous work [29], which demonstrated that surgeon usually feels the operation smoother while burring the bone surface under a higher angular velocity. In addition, there are obviously two stages in both the measured and simulated burring force data. In the first stage, the force value quickly increases. It is related to the contact of the burr to the bone sample in which the contact area is continually changing. This stage is relatively transient. In the second stage, the force value varies within a small range. It is due to the steady burring conditions.

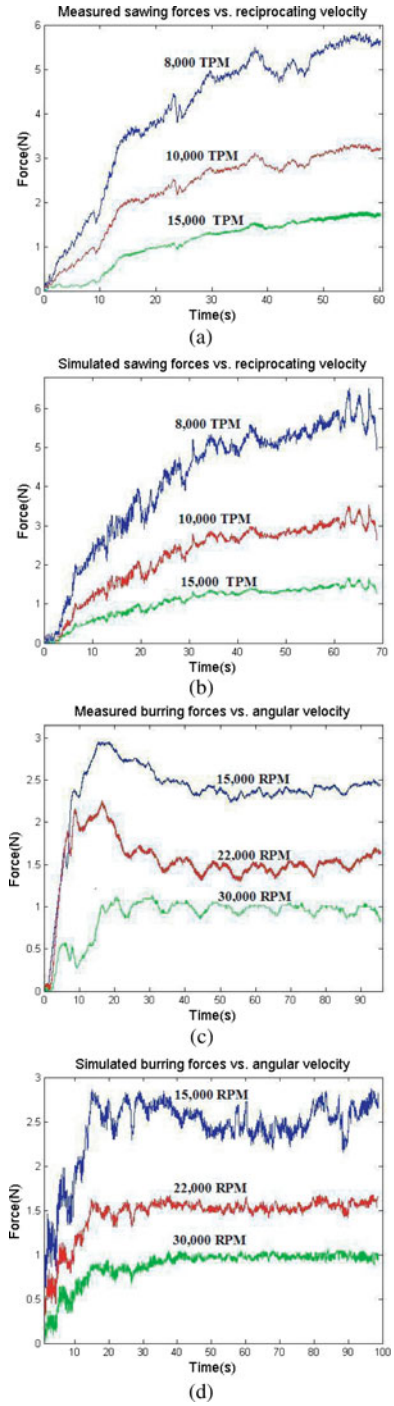

Fig. 7. Comparison of the measured and simulated bone-sawing and bone-burring forces.

From the previous comparisons, we can see that the variations and trends between our simulated sawing/burring forces and the measured ones are similar. Moreover, important features of the measured force data can be found in the simulated force data.

B. Empirical Study

In order to validate that the proposed mandibular angle reduction simulator can enhance the surgical skills of surgeons, an empirical study has been conducted. The patient specific data

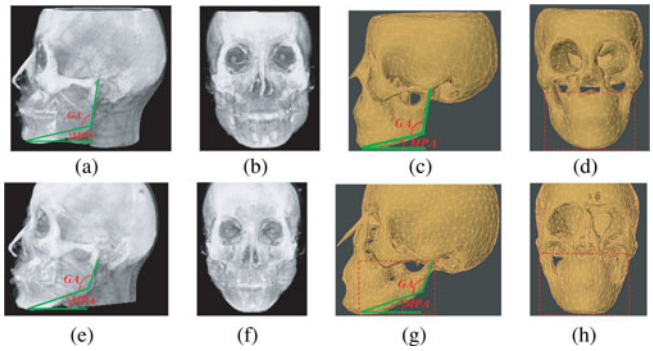

Fig. 8. Patient-specific data.

collected from a hospital were employed as a benchmark compared to the virtual surgery result. A 29-year-old female patient who was dissatisfied with her facial contour sought a treatment for her square-shaped jaw. The lateral view and the anterior view of the full-head CT visualization for the patient before the surgery are shown in Fig. 8(a) and (b). The mandible appearance characteristics can be observed from the corresponding reconstructed skull mesh model in Fig. 8(c) and (d). MPA and GA are the two important angles to measure the mandible in aesthetics. In the anterior view illustrated in Fig. 8(d), the lower face was wide and symmetrical, and GA was 115°, and MPA was 20° in the lateral view, shown in Fig. 8(c).

Mandibular angle reduction was performed on this patient by a senior surgeon. The full-head CT data after the procedure are visualized in Fig. 8(e) and (f) and the corresponding views of the skull model after the surgery are illustrated in Fig. 8(g) and (h). After surgery, the MPA of the patient's mandible was improved to 28° and GA was improved to 126° as shown in Fig. 8(g). As observed in Fig. 8(h), the anterior appearance of the original wide mandible became narrow and symmetrical, the mental region became slick, and the facial proportion was suitable. The contour of mandible margin was smooth and steep from mental region to mandibular angle region. The patient was satisfied with the final result.

Users with two different levels of experience performed the simulated surgical procedure on the patient specific data with the proposed simulator. Fourteen volunteers assigned into two groups were invited to participate this evaluation test. Group one, the novices group, consists of seven novices without any surgery experience. Group two, the expert group, consists of seven resident doctors with relevant experience in orthopedics.

Before performing the virtual surgery, the users were briefed about the procedure with several images and videos from medical books and the Internet, that introduce the techniques of controlling the electric instruments. Furthermore, they were asked to observe a whole surgery process demonstrated by an experienced surgeon. The users were explained the skill of how to achieve better angles of MPA and GA, and how to avoid the dangerous actions that may cause the bone fracture. After some practice to get used to manipulating the haptic device, these two groups were asked to perform the virtual mandibular angle reduction on the patient's model for seven repetitions.

1) Objective Performance Metrics and Comparison: Objective assessment of surgical performance is important in VR-based simulations and these measures have the potential to provide valuable feedback to surgeons to improve their skills. Four key performance metrics were used to evaluate the performance of the users: 1) difference of the GA between the simulated result and the actual surgical result, 2) difference of MPA between the simulated one and the actual result, 3) time the user performed to complete the surgical task, and 4) percentage that the generated sawing torque exceeds the predetermined threshold. The time the user completed the whole task was recorded as the total time for that trial. Since the patient was satisfied with the surgical result and no complications happened during or after the surgery, the result of the actual surgical result served as a benchmark. Consequently, the differences of these two angles were considered to be important when evaluating the proficiency of a surgeon. The percentage was computed as the ratio of the number of the generated torques exceeding the predefined threshold and the total number of the generated torques during each trail. The percentage was considered as the criterion of the safety while the user performs virtual surgery. The surgeon with good skill would avoid those dangerous actions, which may lead to the fracture of the bone or breakage of the instrument.

2) Analysis and Evaluation: The evaluation results is shown in Fig. 9. In Fig. 9(a) and (b), the difference of GA and of MPA with the result from the real treatment for both two groups improves gradually, where the expert group can always obtain a difference within a range of (5.2, 5.6) for GA and (1.6, 1.9) for MPA and the novice group has a wider range of (6.3, 7.4) for GA and (2.2, 2.7) for MPA. In Fig. 9(c), the completion time of the novice group has an obvious drop following the repetition time, while a stable curve could be seen from the completion time of the expert group. Fig. 9(d) clearly illustrates that the expert group operated safer than the novices because the long surgical practice has already helped the experts to keep their hands steady during the surgery. It is observed in Fig. 9 that the expert group outperformed the novice group in terms of the four metrics.

The collected data from the study were further examined using data analysis. Nonparametric analysis (Friedman's test) was carried out for the difference of GA, MPA, the completion time, and the percentage of the torque exceeding the threshold in order to examine the difference between the performance score from each session and the score from consecutive sessions. For difference of GA, curves reached a plateau after the fifth repetition for the novice group and the second repetition for the expert group (Friedman's tests, $P < 0.05$). For the difference of MPA, novices performance decreased after the third repetitions (Friedman's tests, $P < 0.05$), while the expert group did not show significant difference of MPA (Friedman's tests, $P > 0.6$). This demonstrates that training methods are helpful to improve the accuracy of mandibular angle reduction surgery for novices. Furthermore, novices obviously reduced the completion time after the third repetitions (Friedman's tests, $P < 0.05$). Expert surgeons did not show any significant reduction in their completion time (Friedman's tests, $P > 0.65$), demonstrating that our methods can reduce the completion time of novices while it had no obvious effects on experienced surgeons for this aspect. For percentage of the torque exceeding the threshold, curves reached a plateau after the sixth repetition for the novice group

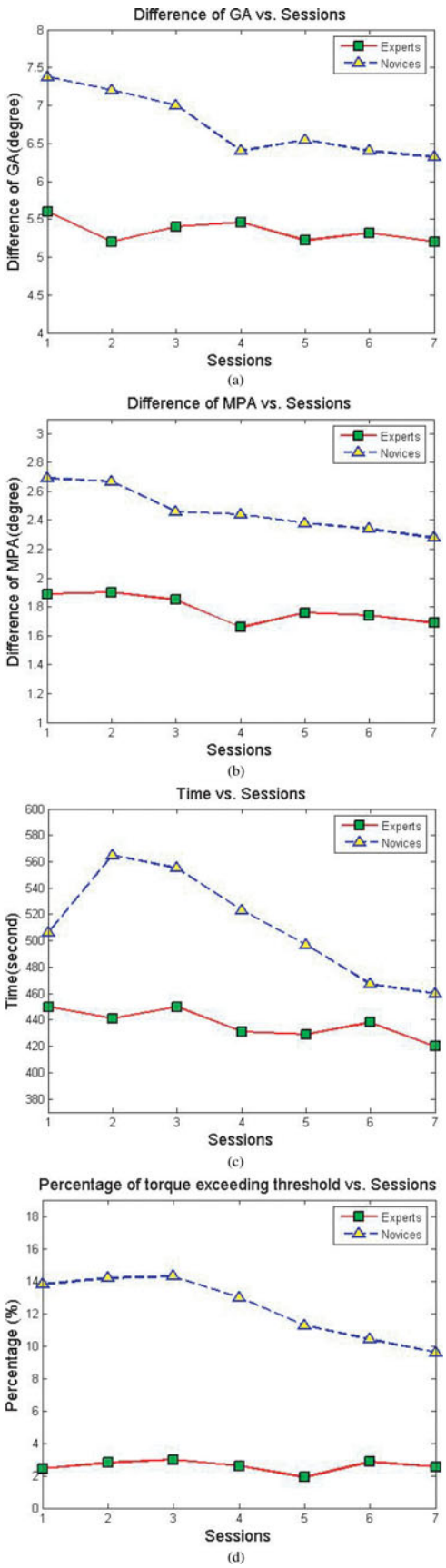

Fig. 9. Learning curves of Group 1 and Group 2 for: (a) difference of GA, (b) difference of MPA, (c) completion time, and (d) percentage of torque exceeding the threshold.

TABLE I
QUESTIONNAIRE ASSESSMENT

Rating	Very good	Good	Fair	Bad	Very bad
spatial 3D perception of the manipulation	100%	0%	0%	0%	0%
reality of the haptic feedback	71.4%	14.2%	14.2%	0%	0%
visual effect of the virtual environment	57.1%	14.2%	28.5%	0%	0%
value of the simulator served as an additional training modality	57.1%	28.5%	14.2%	0%	0%

and the third repetition for the expert group (Friedman's tests, $P < 0.05$).

The seven volunteers in the expert group were also required to assess the simulator by completing a questionnaire after performing the virtual surgery with the proposed simulator. The questionnaire included four basic questions: 1) the spatial 3-D perception of the manipulation, 2) the reality of the haptic feedback, 3) the visual effect of the virtual environment, and 4) the value of the proposed simulator served as an additional training modality. Each question was rated in five levels: very good, good, fair, bad, and very bad. Table I summarizes the results of questionnaire assessment. It shows that almost all the surgeons in the expert group were satisfied with the simulator and recommended the addition of more training procedures in future.

VII. DISCUSSION AND CONCLUSION

This paper demonstrates the construction of a system capable of producing a realistic visual and haptic simulation of the mandibular angle reduction. A procedure composed of linear mandibular angle osteotomy with a reciprocating saw and bone edges smoothing with a round burr was simulated in the system. The proposed method presents an efficient and useful solution for simulating interactions for the two electronic instruments. In the evaluation, actual clinical data were used to compare with the simulated results. In future, we will extend our algorithm to other typical operations in orthopedic surgery such as oscillating sawing, which allows a curved cutting of the bone. Currently, the number of sampled points on the haptic instrument need to be determined by experimental calibration. Therefore, the efficient algorithm to resolve the issue of the simultaneous contact points will be investigated. A study of the intrinsic physical mechanism of the haptic force generation should be conducted. To further evaluate the proposed simulator, we will increase the survey sample size. Moreover, we will continue to develop the quantitative method used to analyze the difference between the real forces collected from the mechanical platform and the simulated forces in our simulator.

REFERENCES

[1] S. K. Kim, J. J. Han, and J. T. Kim, "Classification and treatment of prominent mandibular angle," *Aesthetic Plastic Surg.*, vol. 25, no. 5, pp. 382–387, 2001.

[2] Y. H. Kim, B. C. Cho, and L. J. Lo, "Facial contouring surgery for asians," *Aesthetic Plast Surg.*, vol. 23, no. 1, pp. 22–31, 2009.

[3] D. E. Morris, Z. Moaveni, and L. J. Lo, "Aesthetic facial skeletal contouring in the asian patient," *Division Plastic, Reconstruct., Cosmetic Surg.*, vol. 34, no. 3, pp. 547–556, 2007.
[4] K. Han and J. Kim, "Reduction mandibuloplasty: Ostectomy of the lateral cortex around the mandibular angle," *J. Craniofacial Surg.*, vol. 12, no. 4, pp. 314–325, 2001.
[5] A. A. Kane, L. J. Lo, Y. R. Chen, K. H. Hsu, and M. S. Noordhoff, "The course of the inferior alveolar nerve in the normal human mandibular ramus and in patients presenting for cosmetic reduction of the mandibular angles," *J. Craniofacial Surg.*, vol. 106, no. 5, pp. 1162–1174, 2000.
[6] D. Morris, C. Sewell, F. Barbagli, and K. Salisbury, "Visuohaptic simulation of bone surgery for training and evaluation," *IEEE Trans. Comput. Graph. Appl.*, vol. 26, no. 6, pp. 48–57, Nov./Dec. 2006.
[7] B. Pflesser, A. Petersik, U. Tiede, K. H. Hoehne, and R. Leuwer, "Volume cutting for virtual petrous bone surgery," *Comput. Aided Surg.*, vol. 7, no. 2, pp. 74–83, 2002.
[8] M. Agus, A. Giachetti, E. Gobbetti, G. Zanetti, A. Zorcolo, B. Picasso, and S. S. Franceschini, "A haptic model of a bone-cutting burr," *Stud. Health Technol. Inf.*, vol. 94, pp. 4–10, 2003.
[9] M. D. Tsai, M. S. Hsieh, and C. H. Tsai, "Bone drilling haptic interaction for orthopedic surgical simulator," *Comput. Biol. Med.*, vol. 37, no. 12, pp. 1709–1718, 2007.
[10] T. J. Ko and H. S. Kim, "Mechanistic cutting force model in band sawing," *Int. J. Mach. Tools Manuf.*, vol. 39, pp. 1185–1197, 2006.
[11] S. Haque and S. Srinivasan, "A meta-analysis of the training effectiveness of virtual reality surgical simulators," *IEEE Trans. Inf. Technol. Biomed.*, vol. 10, no. 1, pp. 51–58, Jan. 2006.
[12] S. Hariri, C. Rawn, S. Srivastava, P. Youngblood, and A. Ladd, "Evaluation of a surgical simulator for learning clinical anatomy," *Medical Edu.*, vol. 38, no. 8, pp. 896–902, Aug. 2004.
[13] T. P. Grantcharov, L. Bardram, P. Funch-Jensen, and J. Rosenberg, "Learning curves and impact of previous operative experience on performance on a virtual reality simulator to test laparoscopic surgical skills," *Amer. J. Surg.*, vol. 185, no. 2, pp. 146–149, 2003.
[14] M. Arbabtafti, M. Moghaddam, A. Nahvi, M. Mahvash, B. Richardson, and B. Shirinzadeh, "Physics-based haptic simulation of bone machining," *IEEE Trans. Haptics*, vol. 4, no. 1, pp. 39–50, Jan./Feb. 2010.
[15] I. Oropesa, P. Lamata, P. Snchez-Gonzlez, J. B. Pagador, M. E. Garcła, F. M. Snchez-Margallo, and E. J. Gmez, *Virtual Reality Simulators for Objective Evaluation on Laparoscopic Surgery: Current Trends and Benefits*. Croatia: Intech Open Access Publisher, 2011.
[16] D. M. Okada, A. M. A. de Sousa, R. de Andrade Huertas, and F. A. Suzuki, "Surgical simulator for temporal bone dissection training," *Brazilian J. Otorhinolaryngol.*, vol. 76, no. 5, pp. 575–578, 2010.
[17] B. Panchaphongsaphak, R. Burgkart, and R. Riener, "Three-dimensional touch interface for medical education," *IEEE Trans. Inf. Technol. Biomed.*, vol. 11, no. 3, pp. 251–263, May 2007.
[18] W. E. Lorensen and H. E. Cline, "Marching cubes: A high resolution 3d surface construction algorithm," *Comput. Graph.*, vol. 21, no. 4, pp. 163–169, 1987.
[19] Q. Wang, H. Chen, W. Wu, J. Qin, and P. A. Heng, "Impulse-based rendering methods for haptic simulation of bone-burring," *IEEE Trans. Haptics*, vol. PP, no. 99, p. 1, Available: http://ieeexplore.ieee.org/xpl/login.jsp?tp=&arnumber=6095548&url=http%3A%2F%2Fieeexplore.ieee.org%2Fxpls%2Fabs_all.jsp%3Farnumber%3D6095548
[20] B. Mirtich, "Impulse-based dynamic simulation of rigid body systems," Ph.D. dissertation, Univ. of California at Berkeley, Berkeley, 1996.
[21] G. van den Bergen, G. Van, and D. Bergen, "Efficient collision detection of complex deformable models using aabb trees," *J. Graph. Tools*, vol. 2, pp. 1–13, 1998.
[22] W. C. Hayes and S. M. Perren, "Plate-bone friction in the compression fixation of fractures," *Clin. Orthopaed. Related Res.*, vol. 89, pp. 236–240, 1972.
[23] W. J. Stronge, Ed., *Impact Mechanics*. Cambridge, U.K.: Cambridge Univ. Press, 2000.
[24] E. Guendelman, R. Bridson, and R. Fedkiw, "Nonconvex rigid bodies with stacking," *ACM Trans. Graphics*, vol. 22, no. 3, pp. 871–878, 2003.
[25] G. Wang, J. Li, A. Khadka, Y. Hsu, W. Li, and J. Hu, "Cad/cam and rapid prototyped titanium for reconstruction of ramus defect and condylar fracture caused by mandibular reduction," *Oral Surg., Oral Med., Oral Pathol., Oral Radiol., Endodontol.*, vol. 338, pp. 1–6, 2011.
[26] J. R. Shewchuk, "Delaunay refinement algorithms for triangular mesh generation," *Comput. Geometry Theory Appl.*, vol. 22, pp. 1–3, 2002.
[27] A. Amresh, G. Farin, and A. Razdan, "Adaptive subdivision schemes for triangular meshes," in *Hierarchical and Geometric Methods in Scientific Visualization*. New York: Springer-Verlag, 2002, pp. 319–327.
[28] R. B. Martin, B. B. David, and N. A. Sharkey, *Skeletal Tissue Mechanics*, 1st ed. New York: Springer-Verlag, 1998.
[29] C. H. Jacobs, M. H. Pope, J. T. Berry, and F. Hoaglund, "A study of the bone machining process-drilling," *J. Biomechanics*, vol. 9, pp. 343–349, 1976.

Qiong Wang received the B.S. and M.S. degrees in information science and technology from Shandong University of Science and Technology, Qingdao Shandong Province, China, and the Ph.D. degree in computer science and engineering from The Chinese University of Hong Kong, Shatin, Hong Kong.

She is currently in the Department of Computer Science and Engineering, The Chinese University of Hong Kong. Her research interests include human–computer interaction, haptics, virtual reality, and computer-assisted surgery.

Hui Chen received the B.S. and M.S. degrees in computer science from Shandong University, Shandong, China, and the Ph.D. degree in computer science and engineering from The Chinese University of Hong Kong, Shatin, Hong Kong.

She is currently an Associate Professor in The Intelligence Engineering Lab, Institute of Software, Chinese Academy of Sciences, Beijing, China. Her research interests include human–computer interaction, haptics, virtual reality, and computer-assisted surgery.

Wen Wu (M'11) received the Ph.D. degree in computer science and engineering from The Chinese University of Hong Kong, Shatin, Hong Kong.

She is currently an Assistant Professor in the Department of Computer and Information Science, University of Macau, Macau, China, and an honorary Research Associate in the Department of Computer Science and Engineering, The Chinese University of Hong Kong. Her research interests include medical simulation, virtual reality, and physically based animation.

Hai-Yang Jin received the B.S. degree in mechanical engineering from the Harbin Institute of Technology, Harbin, China, in 2005, and the M.S. degree in mechatronic engineering from Shenzhen Graduate School, Harbin Institute of Technology, China, in 2007, where he is currently working toward the Ph.D. degree in mechatronic engineering. He is currently a guest student at the Shenzhen Institutes of Advanced Technology, Chinese Academy of Science, Beijing, China.

His research interests include the robotic surgical system.

Pheng-Ann Heng (SM'06) received the Ph.D. degree in computer science from Indiana University Bloomington, Bloomington, in 1992.

He is currently a Professor in the Department of Computer Science and Engineering, The Chinese University of Hong Kong, Shatin, China. His research interests include virtual reality applications in medicine, visualization, medical imaging, human–computer interaction, and computer graphics.